

# A note on transformed Fourier systems for the approximation of non-periodic signals

Robert Nasdala<sup>1</sup>

Daniel Potts<sup>2</sup>

A variety of techniques have been developed for the approximation of non-periodic functions. In particular, there are approximation techniques based on rank-1 lattices and transformed rank-1 lattices, including methods that use sampling sets consisting of Chebyshev- and tent-transformed nodes. We compare these methods with a parameterized transformed Fourier system that yields similar  $\ell_2$ -approximation errors.

## 1 Introduction

For the approximation of non-periodic functions defined on the cube  $[0, 1]^d$ , fast algorithms based on Chebyshev- and tent-transformed rank-1 lattice methods have been introduced and studied in [10, 19, 8, 22, 12, 11, 16]. Recently, we suggested a general framework for transformed rank-1 lattice approximation, in which functions defined on a cube  $[0, 1]^d$  (or on  $\mathbb{R}^d$ ) are periodized onto the torus  $\mathbb{T}^d \simeq [0, 1]^d$ , [17, 18]. In these approaches we define parameterized families  $\psi(\cdot, \boldsymbol{\eta}) : [0, 1]^d \rightarrow [0, 1]^d$ ,  $\boldsymbol{\eta} \in \mathbb{R}_+^d$  of transformations that, depending on the parameter choice, yield a certain smoothening effect when composed with a given non-periodic function. This periodization strategies also lead to general parameterized classes of orthonormal systems in weighted Hilbert spaces. However, these methods have the natural drawback of singularities appearing at the boundary points of the cube, so that any approximation error estimates have to be done with respect to weighted  $L_\infty$ - and  $L_2$ -norms.

We summarize some crucial properties of rank-1 lattice approximation. Then, we compare the approximation with a half-periodic cosine system and tent-transformed sampling nodes [13, 3, 1, 2, 22], the Chebyshev approximation [19, 16], as well as the general framework for the parameterized transformed Fourier system [18]. We discuss numerical results in up to dimension  $d = 7$  and highlight the controlled smoothening effect when varying the parameter  $\boldsymbol{\eta}$  in the transformed Fourier systems.

---

<sup>1</sup>Faculty of Mathematics, Chemnitz University of Technology, D-09107 Chemnitz, Germany.  
E-mail: robert.nasdala@math.tu-chemnitz.de

<sup>2</sup>Faculty of Mathematics, Chemnitz University of Technology, D-09107 Chemnitz, Germany.  
E-mail: potts@math.tu-chemnitz.de

## 2 Approximation methods

At first, we summarize the main ideas of the Fourier approximation with sampling sets in the form of rank-1 lattices [21, 7, 14]. Afterwards, we consider Chebyshev- and tent-transformed rank-1 lattices in the context of Chebyshev and cosine approximation methods [22, 16]. Finally, we outline the transformed Fourier system for the approximation of non-periodic signals, as introduced in [18], and provide two examples of parameterized transformations.

### 2.1 Fourier approximation

For any frequency set  $I \subset \mathbb{Z}^d$  of finite cardinality  $|I| < \infty$  we denote the space of all multivariate trigonometric polynomials supported on  $I$  by

$$\Pi_I := \text{span} \left\{ e^{2\pi i \mathbf{k} \cdot \mathbf{x}} = \prod_{\ell=1}^d e^{2\pi i k_\ell x_\ell} : \mathbf{k} = (k_1, \dots, k_d)^\top \in I, \mathbf{x} = (x_1, \dots, x_d)^\top \in \mathbb{T}^d \right\}.$$

Trigonometric polynomials are orthonormal with respect to the  $L_2(\mathbb{T}^d)$ -scalar product

$$(f, g)_{L_2(\mathbb{T}^d)} := \int_{\mathbb{T}^d} f(\mathbf{x}) \overline{g(\mathbf{x})} \, d\mathbf{x}, \quad f, g \in L_2(\mathbb{T}^d).$$

For all  $\mathbf{k} \in \mathbb{Z}^d$  we denote the *Fourier coefficients*  $\hat{h}_{\mathbf{k}}$  by

$$\hat{h}_{\mathbf{k}} := (h, e^{2\pi i \mathbf{k}(\cdot)})_{L_2(\mathbb{T}^d)} = \int_{\mathbb{T}^d} h(\mathbf{x}) e^{-2\pi i \mathbf{k} \cdot \mathbf{x}} \, d\mathbf{x},$$

and the corresponding *Fourier partial sum* by  $S_I h(\mathbf{x}) := \sum_{\mathbf{k} \in I} \hat{h}_{\mathbf{k}} e^{2\pi i \mathbf{k} \cdot \mathbf{x}}$ .

We use sampling nodes in a *rank-1 lattice*  $\Lambda(\mathbf{z}, M)$  of size  $M \in \mathbb{N}$  generated by the vector  $\mathbf{z} \in \mathbb{Z}^d$ , that is defined as

$$\Lambda(\mathbf{z}, M) := \left\{ \mathbf{x}_j^{\text{latt}} := \frac{j}{M} \mathbf{z} \pmod{\mathbf{1}} \in \mathbb{T}^d : j = 0, \dots, M-1 \right\}, \quad (2.1)$$

with  $\mathbf{1} := (1, \dots, 1)^\top$ , which allows the fast evaluation of Fourier partial sums via [14, Algorithm 3.1]. For any frequency set  $I \subset \mathbb{Z}^d$  the *difference set* is given by

$$\mathcal{D}(I) := \{ \mathbf{k} \in \mathbb{Z}^d : \mathbf{k} = \mathbf{k}_1 - \mathbf{k}_2 \text{ with } \mathbf{k}_1, \mathbf{k}_2 \in I \}. \quad (2.2)$$

We define the *reconstructing rank-1 lattice*  $\Lambda(\mathbf{z}, M, I)$  as a rank-1 lattice  $\Lambda(\mathbf{z}, M)$  for which the condition

$$\mathbf{t} \cdot \mathbf{z} \not\equiv 0 \pmod{M} \quad \text{for all } \mathbf{t} \in \mathcal{D}(I) \setminus \{\mathbf{0}\} \quad (2.3)$$

holds. Given a reconstructing rank-1 lattice  $\Lambda(\mathbf{z}, M, I)$ , we have exact integration for all multivariate trigonometric polynomials  $p \in \Pi_{\mathcal{D}(I)}$ , see [21], so that

$$\int_{\mathbb{T}^d} p(\mathbf{x}) \, d\mathbf{x} = \frac{1}{M} \sum_{j=0}^{M-1} p(\mathbf{x}_j), \quad \mathbf{x}_j \in \Lambda(\mathbf{z}, M, I). \quad (2.4)$$

In particular, for  $h \in \Pi_I$  and  $\mathbf{k} \in I$  we have  $h(\cdot) e^{-2\pi i \mathbf{k}(\cdot)} \in \Pi_{\mathcal{D}(I)}$  and

$$\hat{h}_{\mathbf{k}} = \int_{\mathbb{T}^d} h(\mathbf{x}) e^{-2\pi i \mathbf{k} \cdot \mathbf{x}} d\mathbf{x} = \frac{1}{M} \sum_{j=0}^{M-1} h(\mathbf{x}_j) e^{-2\pi i \mathbf{k} \cdot \mathbf{x}_j}, \quad \mathbf{x}_j \in \Lambda(\mathbf{z}, M, I). \quad (2.5)$$

Next, we focus on functions in the Wiener algebra  $\mathcal{A}(\mathbb{T}^d)$  containing all  $L_1(\mathbb{T}^d)$ -functions with absolutely summable Fourier coefficients  $\hat{h}_{\mathbf{k}}$  given by

$$\mathcal{A}(\mathbb{T}^d) := \left\{ h \in L_1(\mathbb{T}^d) : \sum_{\mathbf{k} \in \mathbb{Z}^d} |\hat{h}_{\mathbf{k}}| < \infty \right\}. \quad (2.6)$$

For an arbitrary function  $h \in \mathcal{A}(\mathbb{T}^d) \cap \mathcal{C}(\mathbb{T}^d)$  and lattice points  $\mathbf{x}_j \in \Lambda(\mathbf{z}, M, I)$  we lose the former mentioned exact integration property and get *approximated Fourier coefficients*  $\hat{h}_{\mathbf{k}}^\Lambda$  of the form

$$\hat{h}_{\mathbf{k}} \approx \hat{h}_{\mathbf{k}}^\Lambda := \frac{1}{M} \sum_{j=0}^{M-1} h(\mathbf{x}_j) e^{-2\pi i \mathbf{k} \cdot \mathbf{x}_j}$$

leading to the *approximated Fourier partial sum*  $S_I^\Lambda h$  given by

$$h(\mathbf{x}) \approx S_I^\Lambda h(\mathbf{x}) := \sum_{\mathbf{k} \in I} \hat{h}_{\mathbf{k}}^\Lambda e^{2\pi i \mathbf{k} \cdot \mathbf{x}}.$$

For the matrix-vector-expression with respect to the frequency set  $I_{\text{latt}} \subset \mathbb{Z}^d$  we put

$$\mathbf{F}_{\text{latt}} := \left\{ e^{2\pi i \mathbf{k} \cdot \mathbf{x}_j^{\text{latt}}} \right\}_{j=0, \mathbf{k} \in I_{\text{latt}}}^{M-1}, \quad \mathbf{h}_{\text{latt}} := \left( h(\mathbf{x}_j^{\text{latt}}) \right)_{j=0}^{M-1}.$$

The evaluation of the function  $h$  and the reconstruction of the approximated Fourier coefficients  $\hat{\mathbf{h}} := (\hat{h}_{\mathbf{k}}^\Lambda)_{\mathbf{k} \in I_{\text{latt}}}$  are realized by the fast Algorithms outlined in [14, Algorithm 3.1 and 3.2] that solve the systems

$$\mathbf{h}_{\text{latt}} = \mathbf{F}_{\text{latt}} \hat{\mathbf{h}} \quad \text{and} \quad \hat{\mathbf{h}} = \frac{1}{M} \mathbf{F}_{\text{latt}}^* \mathbf{h}_{\text{latt}}, \quad (2.7)$$

where we have  $\mathbf{F}_{\text{latt}}^* \mathbf{F}_{\text{latt}} = M\mathbf{I}$  by construction with the identity matrix  $\mathbf{I} \in \mathbb{C}^{|I_{\text{latt}}| \times |I_{\text{latt}}|}$ .

## 2.2 Cosine approximation

Next, we consider the half-periodic cosine system

$$\left\{ \lambda_{\mathbf{k}}(\mathbf{x}) := \sqrt{2}^{|\mathbf{k}|_0} \prod_{\ell=1}^d \cos(\pi k_\ell x_\ell) \right\}_{\mathbf{k} \in I_{\text{tent}}}, \quad I_{\text{tent}} \subset \mathbb{N}_0^d, \mathbf{x} \in [0, 1]^d, \quad (2.8)$$

with the zero-norm  $\|\mathbf{k}\|_0 := |\{\ell \in \{1, \dots, d\} : k_\ell \neq 0\}|$  and  $\sqrt{2}^{|\mathbf{k}|_0} := \prod_{\ell=1}^d \sqrt{2}^{|k_\ell|_0}$ . In [13] it is pointed out that this system can alternatively be defined in one dimension over the domain  $t \in [-1, 1]$  as the system  $\lambda_0(x) = \frac{1}{\sqrt{2}}, \lambda_k(t) = \cos(k\pi t), \tilde{\lambda}_k(t) = \sin((k - \frac{1}{2})\pi t)$ , which yields the original cosine system after applying the transformation  $t = 2x - 1$ .

The cosine system (2.8) is orthonormal with respect to the  $L_2([0, 1]^d)$ -scalar product given by

$$(f, g)_{L_2([0, 1]^d)} := \int_{[0, 1]^d} f(\mathbf{x}) \overline{g(\mathbf{x})} \, d\mathbf{x}, \quad f, g \in L_2([0, 1]^d).$$

For  $\mathbf{k} \in \mathbb{Z}^d$  the cosine coefficient of a function  $h \in L_2([0, 1]^d)$  is naturally defined as  $\hat{h}_{\mathbf{k}}^{\text{cos}} := (h, \lambda_{\mathbf{k}})_{L_2([0, 1]^d)}$  and for  $I \subset \mathbb{Z}^d$  the corresponding cosine partial sum is given by  $S_I h(\mathbf{x}) := \sum_{\mathbf{k} \in I} \hat{h}_{\mathbf{k}}^{\text{cos}} \lambda_{\mathbf{k}}(\mathbf{x})$ . We transfer the crucial properties of the Fourier system via the tent transformation

$$\psi(\mathbf{x}) := (\psi_1(x_1), \dots, \psi_d(x_d))^{\top}, \quad \psi_{\ell}(x_{\ell}) = \begin{cases} 2x_{\ell} & \text{for } 0 \leq x_{\ell} < \frac{1}{2}, \\ 2 - 2x_{\ell} & \text{for } \frac{1}{2} \leq x_{\ell} \leq 1. \end{cases} \quad (2.9)$$

We have sampling nodes in the tent-transformed rank-1 lattice  $\Lambda_{\psi}(\mathbf{z}, M)$  defined as

$$\Lambda_{\psi}(\mathbf{z}, M) := \left\{ \mathbf{y}_j^{\text{cos}} := \psi(\mathbf{x}_j^{\text{latt}}) : \mathbf{x}_j^{\text{latt}} \in \Lambda(\mathbf{z}, M), j = 0, \dots, M-1 \right\} \quad (2.10)$$

and we speak of a reconstructing tent-transformed rank-1 lattice  $\Lambda_{\psi}(\mathbf{z}, M, I)$  if the underlying rank-1 lattice is a reconstructing one. Recalling the definition of difference sets  $\mathcal{D}(I)$  in (2.2), multivariate trigonometric polynomials  $h(\cdot)$ ,  $\lambda_{\mathbf{k}}(\cdot)$  and  $\lambda_{\mathbf{k}}(\cdot)$  that are in  $\Pi_{\mathcal{D}(I)}$  and supported on  $\mathbf{k} \in I \subset \mathbb{N}_0^d$  inherit the exact integration property (2.4), because with the tent transformation as in (2.9) and transformed nodes  $\mathbf{y}_j^{\text{cos}} = \psi(\mathbf{x}_j^{\text{latt}}) \in \Lambda_{\psi}(\mathbf{z}, M, I)$  with  $\mathbf{x}_j^{\text{latt}} = (x_1^j, \dots, x_d^j)^{\top} \in \Lambda(\mathbf{z}, M, I)$  we have

$$\begin{aligned} \hat{h}_{\mathbf{k}}^{\text{cos}} &= \int_{[0, 1]^d} h(\mathbf{y}) \lambda_{\mathbf{k}}(\mathbf{y}) \, d\mathbf{y} = \sqrt{2}^{|\mathbf{k}|_0} \int_{\mathbb{T}^d} h(\psi(\mathbf{x})) \prod_{\ell=1}^d \cos(2\pi k_{\ell} x_{\ell}) \, d\mathbf{x} \\ &= \frac{\sqrt{2}^{|\mathbf{k}|_0}}{2^d} \int_{\mathbb{T}^d} h(\psi(\mathbf{x})) \left( e^{2\pi i \mathbf{k} \cdot \mathbf{x}} + e^{-2\pi i \mathbf{k} \cdot \mathbf{x}} \right) \, d\mathbf{x} \\ &= \frac{\sqrt{2}^{|\mathbf{k}|_0}}{2^d} \frac{1}{M} \sum_{j=0}^{M-1} h(\psi(\mathbf{x}_j)) \left( e^{2\pi i \mathbf{k} \cdot \mathbf{x}_j} + e^{-2\pi i \mathbf{k} \cdot \mathbf{x}_j} \right) \\ &= \sqrt{2}^{|\mathbf{k}|_0} \frac{1}{M} \sum_{j=0}^{M-1} h(\psi(\mathbf{x}_j)) \prod_{\ell=1}^d \cos(2\pi k_{\ell} x_{\ell}^j) \\ &= \frac{1}{M} \sum_{j=0}^{M-1} h(\mathbf{y}_j^{\text{cos}}) \lambda_{\mathbf{k}}(\mathbf{y}_j^{\text{cos}}). \end{aligned}$$

For an arbitrary function  $h \in \mathcal{C}([0, 1]^d)$ , we lose the former mentioned exactness and define the *approximated cosine coefficients*  $\hat{h}_{\mathbf{k}}^{\text{cos}, \Lambda}$  of the form

$$\hat{h}_{\mathbf{k}}^{\text{cos}} \approx \hat{h}_{\mathbf{k}}^{\text{cos}, \Lambda} := \frac{1}{M} \sum_{j=0}^{M-1} h(\mathbf{y}_j^{\text{cos}}) \lambda_{\mathbf{k}}(\mathbf{y}_j^{\text{cos}}), \quad \mathbf{y}_j^{\text{cos}} \in \Lambda_{\psi}(\mathbf{z}, M, I),$$

and obtain *approximated cosine partial sum*  $S_I^{\Lambda} h$  given by

$$h(\mathbf{x}) \approx S_I^{\Lambda} h(\mathbf{x}) := \sum_{\mathbf{k} \in I} \hat{h}_{\mathbf{k}}^{\text{cos}, \Lambda} \lambda_{\mathbf{k}}(\mathbf{x}). \quad (2.11)$$

In matrix-vector-notation we have

$$\mathbf{C} := \left\{ \lambda_{\mathbf{k}} \left( \mathbf{y}_j^{\cos} \right) \right\}_{j=0, \mathbf{k} \in I_{\text{tent}}}^{M-1}, \quad \mathbf{h}_{\text{tent}} := \left( h \left( \mathbf{y}_j^{\cos} \right) \right)_{j=0}^{M-1}.$$

Both the evaluation of  $h$  and the reconstruction of the approximated cosine coefficients  $\hat{\mathbf{h}} := \left\{ \hat{h}_{\mathbf{k}}^{\cos, \Lambda} \right\}_{\mathbf{k} \in I_{\text{tent}}}$  is realized by solving the systems

$$\mathbf{h}_{\text{tent}} = \mathbf{C} \hat{\mathbf{h}} \quad \text{and} \quad \hat{\mathbf{h}} = \frac{1}{M} \mathbf{C}^* \mathbf{h}_{\text{tent}}, \quad (2.12)$$

where we have  $\mathbf{C}^* \mathbf{C} = M \mathbf{I}$  by construction with the identity matrix  $\mathbf{I} \in \mathbb{C}^{|I_{\text{tent}}| \times |I_{\text{tent}}|}$ . Fast algorithms for solving both systems are described in [22, 16].

### 2.3 Chebyshev approximation

We consider the Chebyshev system, that is defined for  $\mathbf{x} \in [0, 1]^d$  and a finite frequency set  $I_{\text{cheb}} \subset \mathbb{N}_0^d$  as

$$\left\{ T_{\mathbf{k}}(\mathbf{x}) := \sqrt{2}^{\|\mathbf{k}\|_0} \prod_{\ell=1}^d \cos(k_{\ell} \arccos(2x_{\ell} - 1)) \right\}_{\mathbf{k} \in I_{\text{cheb}}}. \quad (2.13)$$

The Chebyshev system (2.13) is an orthonormal system with respect to the weighted scalar product

$$(T_{\mathbf{k}_1}, T_{\mathbf{k}_2})_{L_2([0, 1]^d, \omega)} := \int_{[0, 1]^d} T_{\mathbf{k}_1}(\mathbf{x}) T_{\mathbf{k}_2}(\mathbf{x}) \omega(\mathbf{x}) \, d\mathbf{x}, \quad \omega(\mathbf{x}) := \prod_{\ell=1}^d \frac{2}{\pi \sqrt{4x_{\ell}(1-x_{\ell})}}.$$

The *Chebyshev coefficients* of a function  $h \in L_2([0, 1]^d, \omega)$  are naturally defined as  $\hat{h}_{\mathbf{k}}^{\text{cheb}} := (h, T_{\mathbf{k}})_{L_2([0, 1]^d, \omega)}$ ,  $\mathbf{k} \in \mathbb{Z}^d$  and for  $I \subset \mathbb{Z}^d$  the corresponding Chebyshev partial sum is given by  $S_I h(\mathbf{x}) := \sum_{\mathbf{k} \in I} \hat{h}_{\mathbf{k}}^{\text{cheb}} T_{\mathbf{k}}(\mathbf{x})$ . We transfer some properties of the Fourier system via the *Chebyshev transformation*

$$\psi(\mathbf{x}) := (\psi_1(x_1), \dots, \psi_d(x_d))^{\top}, \quad \psi_{\ell}(x_{\ell}) := \frac{1}{2} + \frac{1}{2} \cos \left( 2\pi \left( x_{\ell} - \frac{1}{2} \right) \right), \quad x_{\ell} \in [0, 1]. \quad (2.14)$$

We have sampling nodes in the Chebyshev-transformed rank-1 lattice  $\Lambda_{\psi}(\mathbf{z}, M)$  defined as

$$\Lambda_{\psi}(\mathbf{z}, M) := \left\{ \mathbf{y}_j^{\text{cheb}} := \psi \left( \mathbf{x}_j^{\text{latt}} \right) : \mathbf{x}_j^{\text{latt}} \in \Lambda(\mathbf{z}, M), j = 0, \dots, M-1 \right\}. \quad (2.15)$$

It inherits the reconstruction property (2.3) of the underlying reconstructing rank-1 lattice  $\Lambda(\mathbf{z}, M, I)$  and is denoted by  $\Lambda_{\psi}(\mathbf{z}, M, I)$ . We note that Chebyshev transformed sampling nodes are fundamentally connected to Padua points and Lissajous curves, as well as certain interpolation methods that are outlined in [4, 9].

Recalling the definition of difference sets  $\mathcal{D}(I)$  in (2.2), multivariate trigonometric polynomials  $h(\cdot)$  and  $h(\cdot) T_{\mathbf{k}}(\cdot)$  are in  $\Pi_{\mathcal{D}(I)}$  and supported on  $\mathbf{k} \in I \subset \mathbb{N}_0^d$  inherit the exact integration property (2.4), because with the Chebyshev transformation  $\psi$  as in (2.14) and

transformed nodes  $\mathbf{y}_j^{\text{cheb}} = \psi(\mathbf{x}_j^{\text{latt}}) \in \Lambda_\psi(\mathbf{z}, M, I)$  with  $\mathbf{x}_j^{\text{latt}} = (x_1^j, \dots, x_d^j)^\top \in \Lambda(\mathbf{z}, M, I)$  we have

$$\begin{aligned}
\hat{h}_{\mathbf{k}}^{\text{cheb}} &= \int_{[0,1]^d} h(\mathbf{y}) T_{\mathbf{k}}(\mathbf{y}) \omega(\mathbf{y}) \, d\mathbf{y} = \sqrt{2}^{\|\mathbf{k}\|_0} \int_{\mathbb{T}^d} h(\psi(\mathbf{x})) \prod_{\ell=1}^d \cos(2\pi k_\ell x_\ell) \, d\mathbf{x} \\
&= \frac{\sqrt{2}^{\|\mathbf{k}\|_0}}{2^d} \int_{\mathbb{T}^d} h(\psi(\mathbf{x})) \left( e^{2\pi i \mathbf{k} \cdot \mathbf{x}} + e^{-2\pi i \mathbf{k} \cdot \mathbf{x}} \right) \, d\mathbf{x} \\
&= \frac{\sqrt{2}^{\|\mathbf{k}\|_0}}{2^d} \frac{1}{M} \sum_{j=0}^{M-1} h(\psi(\mathbf{x}_j)) \left( e^{2\pi i \mathbf{k} \cdot \mathbf{x}_j} + e^{-2\pi i \mathbf{k} \cdot \mathbf{x}_j} \right) \\
&= \sqrt{2}^{\|\mathbf{k}\|_0} \frac{1}{M} \sum_{j=0}^{M-1} h(\psi(\mathbf{x}_j)) \prod_{\ell=1}^d \cos(2\pi k_\ell x_\ell^j) \\
&= \frac{1}{M} \sum_{j=0}^{M-1} h(\mathbf{y}_j^{\text{cheb}}) T_{\mathbf{k}}(\mathbf{y}_j^{\text{cheb}}).
\end{aligned}$$

For an arbitrary function  $h \in L([0, 1]^d, \omega) \cap \mathcal{C}([0, 1]^d)$ , we lose the former mentioned exactness and define the *approximated Chebyshev coefficients*  $\hat{h}_{\mathbf{k}}^{\text{cheb}, \Lambda}$  of the form

$$\hat{h}_{\mathbf{k}}^{\text{cheb}} \approx \hat{h}_{\mathbf{k}}^{\text{cheb}, \Lambda} := \frac{1}{M} \sum_{j=0}^{M-1} h(\mathbf{y}_j^{\text{cheb}}) T_{\mathbf{k}}(\mathbf{y}_j^{\text{cheb}}), \quad \mathbf{y}_j^{\text{cheb}} \in \Lambda_\psi(\mathbf{z}, M, I),$$

leading to the *approximated Chebyshev partial sum*

$$h(\mathbf{x}) \approx S_I^\Lambda h(\mathbf{x}) := \sum_{\mathbf{k} \in I} \hat{h}_{\mathbf{k}}^{\text{cheb}, \Lambda} T_{\mathbf{k}}(\mathbf{x}). \quad (2.16)$$

In matrix-vector-notation this reads as

$$\mathbf{T} := \left\{ T_{\mathbf{k}}(\mathbf{y}_j^{\text{cheb}}) \right\}_{j=0, \mathbf{k} \in I_{\text{cheb}}}^{M-1}, \quad \mathbf{h}_{\text{cheb}} := \left( h(\mathbf{y}_j^{\text{cheb}}) \right)_{j=0}^{M-1}.$$

The evaluation of  $h$  as well as the reconstruction of the approximated Chebyshev coefficients  $\hat{\mathbf{h}} := \left( \hat{h}_{\mathbf{k}}^{\text{cheb}, \Lambda} \right)_{\mathbf{k} \in I_{\text{cheb}}}$  of  $h$  are realized by fast Algorithms outlined in [19, 22, 16], that solve the systems

$$\mathbf{h}_{\text{cheb}} = \mathbf{T} \hat{\mathbf{h}} \quad \text{and} \quad \hat{\mathbf{h}} = \frac{1}{M} \mathbf{T}^* \mathbf{h}_{\text{cheb}}, \quad (2.17)$$

where we have  $\mathbf{T}^* \mathbf{T} = M \mathbf{I}$  by construction with the identity matrix  $\mathbf{I} \in \mathbb{C}^{|I_{\text{cheb}}| \times |I_{\text{cheb}}|}$ .

## 2.4 Transformed Fourier approximation

We recall the ideas of a particular family of parameterized torus-to-cube transformations as suggested in [18], that generalize the construction idea of the Chebyshev system in composing a mapping with a multiple of its inverse.

We call a continuously differentiable, strictly increasing mapping  $\tilde{\psi} : (0, 1) \rightarrow \mathbb{R}$  with  $\tilde{\psi}(x + \frac{1}{2})$  being odd and  $\tilde{\psi}(x) \rightarrow \pm\infty$  for  $x \rightarrow \{0, 1\}$  a *torus-to- $\mathbb{R}$  transformation*. We obtain a

parameterized *torus-to-cube transformation*  $\psi(\cdot, \eta) : [0, 1] \rightarrow [0, 1]$  with  $\eta \in \mathbb{R}_+ := (0, \infty)$  by putting

$$\psi(x, \eta) := \begin{cases} 0 & \text{for } x = 0, \\ \tilde{\psi}^{-1}(\eta \tilde{\psi}(x)) & \text{for } x \in (0, 1), \\ 1 & \text{for } x = 1, \end{cases} \quad (2.18)$$

which are continuously differentiable, increasing and have a first derivative  $\psi'(\cdot, \eta) \in \mathcal{C}_0([0, 1])$ , where  $\mathcal{C}_0([0, 1])$  denotes the space of all continuous functions vanishing to 0 towards their boundary points. It holds  $\psi^{-1}(y, \eta) = \psi\left(y, \frac{1}{\eta}\right)$  and we call  $\varrho(y, \eta) := (\psi^{-1})'(y, \eta) = \psi'\left(y, \frac{1}{\eta}\right)$  the *density* of  $\psi$ . In multiple dimensions  $d \in \mathbb{N}$  with  $\boldsymbol{\eta} = (\eta_1, \dots, \eta_d)^\top$  we put

$$\begin{aligned} \psi(\mathbf{x}, \boldsymbol{\eta}) &:= (\psi_1(x_1, \eta_1), \dots, \psi_d(x_d, \eta_d))^\top, \\ \psi^{-1}(\mathbf{y}, \boldsymbol{\eta}) &:= (\psi_1^{-1}(y_1, \eta_1), \dots, \psi_d^{-1}(y_d, \eta_d))^\top, \\ \varrho(\mathbf{y}, \boldsymbol{\eta}) &:= \prod_{\ell=1}^d \varrho_\ell(y_\ell, \eta_\ell) \quad \text{with} \quad \varrho_\ell(y_\ell, \eta_\ell) := \frac{1}{\psi'(\psi^{-1}(y_\ell, \eta_\ell))}, \end{aligned} \quad (2.19)$$

where the univariate torus-to-cube transformations  $\psi_\ell(\cdot, \eta_\ell)$  and their corresponding densities  $\varrho_\ell(\cdot, \eta_\ell)$  may be different in each coordinate  $\ell \in \{1, \dots, d\}$ .

We consider integrable weight functions

$$\omega(\mathbf{y}) := \prod_{\ell=1}^d \omega_\ell(y_\ell), \quad \mathbf{y} \in [0, 1]^d,$$

such that for any given torus-to-cube transformation  $\psi(\cdot, \boldsymbol{\eta})$  as in (2.19) we have

$$\omega(\psi_\ell(\cdot, \eta_\ell))\psi'(\cdot, \eta_\ell) \in \mathcal{C}_0([0, 1]).$$

Applying a torus-to-cube transformation to a function  $h \in L_2([0, 1]^d, \omega) \cap \mathcal{C}([0, 1]^d)$  generates a periodic function  $f \in L_2(\mathbb{T}^d)$  of the form

$$f(\mathbf{x}) := h(\psi(\mathbf{x}, \boldsymbol{\eta})) \sqrt{\omega(\psi(\mathbf{x}, \boldsymbol{\eta})) \prod_{\ell=1}^d \psi'_\ell(x_\ell)} \quad \text{with} \quad \|h\|_{L_2([0, 1]^d, \omega)} = \|f\|_{L_2(\mathbb{T}^d)}, \quad (2.20)$$

that is approximated by the classical Fourier system. To construct an approximant for the original function  $h$  we apply the inverse torus-to-cube transformation to the Fourier system, yielding for a fixed  $\boldsymbol{\eta} \in \mathbb{R}_+^d$  the *transformed Fourier system*

$$\left\{ \varphi_{\mathbf{k}}(\cdot) := \sqrt{\frac{\varrho(\cdot, \boldsymbol{\eta})}{\omega(\cdot)}} e^{2\pi i \mathbf{k} \cdot \psi^{-1}(\cdot, \boldsymbol{\eta})} \right\}_{\mathbf{k} \in I}, \quad (2.21)$$

which forms an orthonormal system with respect to the weighted  $L_2([0, 1]^d, \omega)$ -scalar product. For all  $\mathbf{k} \in \mathbb{Z}^d$  the *transformed Fourier coefficients*  $\hat{h}_{\mathbf{k}}$  are naturally defined as

$$\hat{h}_{\mathbf{k}} := (h, \varphi_{\mathbf{k}})_{L_2([0, 1]^d, \omega)} = \int_{[0, 1]^d} h(\mathbf{y}) \overline{\varphi_{\mathbf{k}}(\mathbf{y})} \omega(\mathbf{y}) \, d\mathbf{y},$$

and the corresponding *Fourier partial sum* is given by  $S_I h(\mathbf{y}) := \sum_{\mathbf{k} \in I} \hat{h}_{\mathbf{k}} \varphi(\mathbf{y})$ . The corresponding sampling nodes will be taken from the torus-to-cube-transformed (abbreviated: ttc) rank-1 lattice  $\Lambda_\psi(\mathbf{z}, M)$  defined as

$$\Lambda_\psi(\mathbf{z}, M) := \left\{ \mathbf{y}_j^{\text{ttc}} := \psi \left( \mathbf{x}_j^{\text{latt}}, \boldsymbol{\eta} \right) : \mathbf{x}_j^{\text{latt}} \in \Lambda(\mathbf{z}, M), j = 0, \dots, M-1 \right\} \quad (2.22)$$

and we speak of a reconstructing torus-to-cube-transformed rank-1 lattice  $\Lambda_\psi(\mathbf{z}, M, I)$  if the underlying rank-1 lattice is a reconstructing one.

Furthermore, the multivariate transformed trigonometric polynomials supported on  $I \subset \mathbb{Z}^d$  are given by  $\Pi_I^{\text{ttc}} := \text{span}\{\varphi_{\mathbf{k}} : \mathbf{k} \in I\}$  and inherit the exact integration property (2.5), thus, for  $h \in \Pi_I^{\text{ttc}}$  we have

$$\hat{h}_{\mathbf{k}} = \int_{[0,1]^d} h(\mathbf{x}) \varphi_{\mathbf{k}}(\mathbf{x}) \, d\mathbf{x} = \frac{1}{M} \sum_{j=0}^{M-1} h(\mathbf{y}_j^{\text{ttc}}) \varphi_{\mathbf{k}}(\mathbf{y}_j^{\text{ttc}}), \quad \mathbf{y}_j^{\text{ttc}} \in \Lambda_\psi(\mathbf{z}, M, I).$$

For an arbitrary function  $h \in L_2([0,1]^d, \omega) \cap \mathcal{C}([0,1]^d)$  we lose the former mentioned exactness and define approximated transformed coefficients of the form

$$\hat{h}_{\mathbf{k}}^\Lambda := \frac{1}{M} \sum_{j=0}^{M-1} h(\mathbf{y}_j^{\text{ttc}}) \varphi_{\mathbf{k}}(\mathbf{y}_j^{\text{ttc}})$$

and leads to the *approximated transformed Fourier partial sum*  $S_I^\Lambda h$  given by

$$h(\mathbf{y}) \approx S_I^\Lambda h(\mathbf{y}) := \sum_{\mathbf{k} \in I} \hat{h}_{\mathbf{k}}^\Lambda \varphi_{\mathbf{k}}(\mathbf{y}). \quad (2.23)$$

In matrix-vector-notation we have

$$\mathbf{h}_{\text{ttc}} := (h(\mathbf{y}_j^{\text{ttc}}))_{j=0}^{M-1}, \quad \mathbf{F}_{\text{ttc}} := \{\varphi_{\mathbf{k}}(\mathbf{y}_j^{\text{ttc}})\}_{j=0, \mathbf{k} \in I_{\text{ttc}}}^{M-1}.$$

The evaluation of  $h$  and the reconstruction of the approximated transformed Fourier coefficients  $\hat{\mathbf{h}} := \{\hat{h}_{\mathbf{k}}^\Lambda\}_{\mathbf{k} \in I_{\text{ttc}}}$  is realized by solving the systems

$$\mathbf{h}_{\text{ttc}} = \mathbf{F}_{\text{ttc}} \hat{\mathbf{h}}. \quad \text{and} \quad \hat{\mathbf{h}} = \frac{1}{M} \mathbf{F}_{\text{ttc}}^* \mathbf{h}_{\text{ttc}}. \quad (2.24)$$

Fast algorithms for solving both systems are described in [18].

## 2.5 Comparison of the orthonormal systems

The previously presented approximation approaches are based on very different orthonormal systems and use differently transformed sampling sets, which is summarized in dimension  $d = 1$  in Table 2.1 with the definition of the hyperbolic cross  $I_N^1$  given in (3.1).

Given an univariate continuous function  $h \in \mathcal{C}([0,1])$ , both composition with the tent transformation (2.9) and the Chebyshev transformation (2.14) can be interpreted as mirroring a compressed version of  $h$  at the point  $\frac{1}{2}$ , so that  $h(\psi(x)) = h(\psi(1-x))$  for all  $x \in [0, \frac{1}{2}]$ . In contrast to the the Chebyshev transformation case, for the tent transformation we generally



won't expect the resulting function  $h \circ \psi$  to be smooth at the point  $\frac{1}{2}$ , which will be reflected in the approximation results later on.

The parametrized torus-to-cube transformations (2.18) are a fundamentally different transformation class in the sense that the periodization effect is caused primarily by the multiplication of  $h(\psi(\cdot, \eta))$  with the first derivative  $\psi(\cdot, \eta) \in \mathcal{C}_0([0, 1])$  (assuming a constant weight function  $\omega \equiv 1$ ), so that the function  $h(\psi(\cdot, \eta))\sqrt{\psi(\cdot, \eta)}$  ends up being continuously extendable to the torus  $\mathbb{T}$ . Additionally, now there is the parameter  $\eta$  involved which controls the smoothening effect on the periodized function, see [18].

**Example 2.1.** We find various suggestions for torus-to- $\mathbb{R}$  transformations in [5, Section 17.6], [20, Section 7.5] and [17]. We list some induced combined transformations  $\psi(x, \eta)$  and the corresponding density function  $\varrho(y, \eta) = (\psi^{-1})'(y, \eta)$  in the sense of definition (2.18):

- the logarithmic torus-to-cube transformation

$$\psi(x, \eta) := \frac{1}{2} + \frac{1}{2} \tanh(\eta \tanh^{-1}(2x - 1)), \quad \varrho(y, \eta) = \frac{4}{\eta} \frac{(4y - 4y^2)^{\frac{1}{\eta} - 1}}{\left((2y)^{\frac{1}{\eta}} + (2 - 2y)^{\frac{1}{\eta}}\right)^2}, \quad (2.25)$$

based on the mapping

$$\tilde{\psi}(x) = \frac{1}{2} \log \left( \frac{2x}{2 - 2x} \right) = \tanh^{-1}(2x - 1),$$

- the error function torus-to-cube transformation

$$\psi(x, \eta) = \frac{1}{2} \operatorname{erf}(\eta \operatorname{erf}^{-1}(2x - 1)) + \frac{1}{2}, \quad \varrho(y, \eta) = \frac{1}{\eta} e^{(1 - \frac{1}{\eta^2})(\operatorname{erf}^{-1}(2y - 1))^2}, \quad (2.26)$$

based on the mapping

$$\tilde{\psi}(x) = \operatorname{erf}^{-1}(2x - 1),$$

which is the inverse of the error function

$$\operatorname{erf}(y) = \frac{1}{\sqrt{\pi}} \int_{-y}^y e^{-t^2} dt, \quad y \in \mathbb{R},$$

□

In Figure 2.1 we provide a side-by-side comparison of all the previously mentioned transformation mappings.

### 3 Approximation results and error analysis

Based on the weight function

$$\omega_{\text{hc}}(\mathbf{k}) := \prod_{\ell=1}^d \max(1, |k_\ell|), \quad \mathbf{k} \in \mathbb{Z}^d,$$

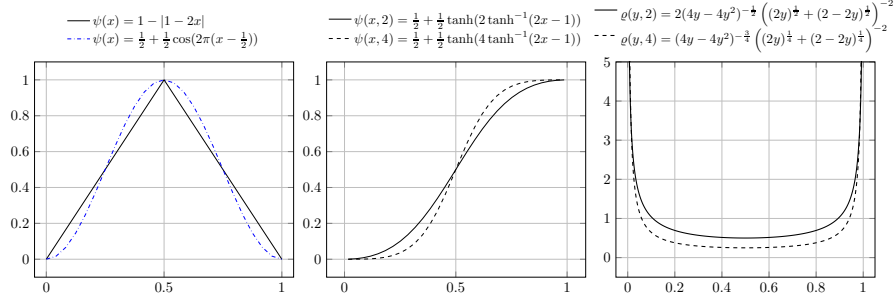


Figure 2.1: Left: The tent-transformation (2.9) the Chebyshev-transformation (2.14). Center and right: The parameterized logarithmic transformation (2.25) and its density function for  $\eta \in \{2, 4\}$ .

orthonormal system $\{\varphi_k(x)\}_{k \in I}$	scalar product weight $\omega$	sampling transformation $\psi$	frequency set $I$
$\sqrt{2}^{\ k\ _0} \cos(\pi k x)$	1	$\begin{cases} 2x & \text{for } 0 \leq x < \frac{1}{2}, \\ 2 - 2x & \text{for } \frac{1}{2} \leq x \leq 1. \end{cases}$	$I_N^d \cap \mathbb{N}_0^d$
$\sqrt{2}^{\ k\ _0} \cos(k \arccos(2x - 1))$	$\frac{1}{2\pi\sqrt{x(1-x)}}$	$\frac{1}{2} + \frac{1}{2} \cos(2\pi(x - \frac{1}{2}))$	$I_N^d \cap \mathbb{N}_0^d$
$\sqrt{\frac{\varrho(x, \eta)}{\omega(x)}} e^{2\pi i k \psi^{-1}(x, \eta)}$	$\omega(x)$	$\psi(x, \eta)$	$I_N^d$

Table 2.1: Comparison of the univariate orthonormal system, sampling sets and frequency sets from the Chebyshev, cosine and transformed Fourier approximation methods.

we define the hyperbolic cross index set

$$I_N^d := \left\{ \mathbf{k} \in \mathbb{Z}^d : \omega_{\text{hc}}(\mathbf{k}) \leq N \right\} \quad (3.1)$$

and for  $\beta \geq 0$  we furthermore have the Hilbert spaces

$$\mathcal{H}^\beta(\mathbb{T}^d) := \left\{ f \in L_2(\mathbb{T}^d) : \|f\|_{\mathcal{H}^\beta(\mathbb{T}^d)} := \left( \sum_{\mathbf{k} \in \mathbb{Z}^d} \omega_{\text{hc}}(\mathbf{k})^{2\beta} |\hat{f}_{\mathbf{k}}|^2 \right)^{\frac{1}{2}} < \infty \right\} \quad (3.2)$$

that are closely related to the Wiener Algebra  $\mathcal{A}(\mathbb{T}^d)$  given in (2.6). For  $\lambda > \frac{1}{2}$  and fixed  $d \in \mathbb{N}$  the continuous embeddings  $\mathcal{H}^{\beta+\lambda}(\mathbb{T}^d) \hookrightarrow \mathcal{A}(\mathbb{T}^d)$  was shown in [15, Lemma 2.2]. Next, we introduce the analogue on the cube  $[0, 1]^d$  for the Hilbert space  $\mathcal{H}^\beta(\mathbb{T}^d)$  as in (3.2). We define the space of weighted  $L_2([0, 1]^d, \omega)$ -functions with square summable Fourier coefficients  $\hat{h}_{\mathbf{k}} := (h, \varphi_{\mathbf{k}})_{L_2([0, 1]^d, \omega)}$  by

$$\mathcal{H}^\beta([0, 1]^d, \omega) := \left\{ h \in L_2([0, 1]^d, \omega) : \|h\|_{\mathcal{H}^\beta([0, 1]^d, \omega)} := \left( \sum_{\mathbf{k} \in \mathbb{Z}^d} \omega_{\text{hc}}(\mathbf{k})^{2\beta} |\hat{h}_{\mathbf{k}}|^2 \right)^{\frac{1}{2}} < \infty \right\}. \quad (3.3)$$

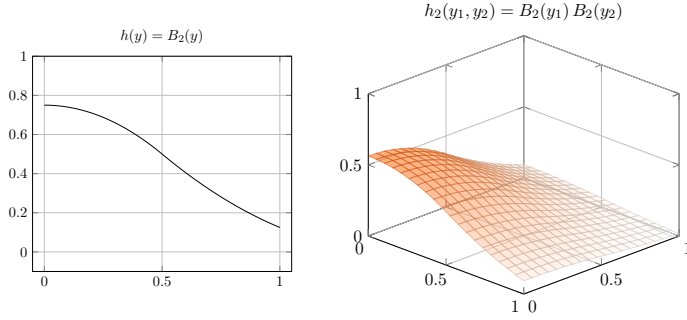


Figure 3.1: The univariate B-spline  $h(y) = B_2(y)$  and the two-dimensional tensor product B-spline  $h_2(y_1, y_2) = B_2(y_1) B_2(y_2)$ .

In case of a constant weight function  $\omega \equiv 1$  we just write  $\mathcal{H}^\beta([0, 1]^d)$ .

We define a shifted, scaled and dilated B-spline of second order as

$$B_2(x) := \begin{cases} -x^2 + \frac{3}{4} & \text{for } 0 \leq x < \frac{1}{2}, \\ \frac{1}{2}(x^2 - 3x + \frac{9}{4}) & \text{for } \frac{1}{2} \leq x \leq 1, \end{cases} \quad (3.4)$$

which we refer to as the  $B_2$ -cutoff, that was also used in [19, 18]. It is in  $\mathcal{C}^1([0, 1])$  and depicted in Figure 3.1. Even though it is only once continuously differentiable, it is also an element in  $\mathcal{H}^{\frac{5}{2}-\varepsilon}([0, 1])$  for any  $\varepsilon > 0$ , which the following arguments show. It's well-known a second order B-spline is the result of a convolution of three step functions  $\chi_{[0,1]}$  (where  $\chi$  denotes the indicator function) with themselves, whose respective Fourier coefficients  $(\chi_{[0,1]}(\cdot), e^{2\pi i k(\cdot)})_{L_2([0,1])}$  decay like  $|k|^{-1}$  for  $k \rightarrow \pm\infty$ . Hence, the Fourier coefficients  $\hat{h}_k = (B_2, e^{2\pi i k(\cdot)})_{L_2([0,1])}$  of the  $B_2$ -cutoff (3.4) decay like  $|k|^{-3}$  for  $k \rightarrow \pm\infty$ . Considering a constant weight function  $\omega \equiv 1$ , the  $\|\cdot\|_{\mathcal{H}^\beta([0,1])}$ -norm given in (3.3) of  $B_2$  is finite if

$$\|B_2\|_{\mathcal{H}^\beta([0,1])}^2 = \sum_{k \in \mathbb{Z}} \omega_{\text{hc}}(k)^{2\beta} |\hat{h}_k|^2 \lesssim \sum_{k \in \mathbb{Z}} \max\{1, |k|\}^{2\beta} \frac{1}{|k|^6} < \infty,$$

which is the case for

$$|k|^{2\beta-6} \leq k^{-(1+\varepsilon)} \Leftrightarrow \beta \leq \frac{5}{2} - \varepsilon, \quad \varepsilon > 0.$$

Next, we approximate the tensor product  $B_2$ -cutoff

$$h(\mathbf{x}) = \prod_{\ell=1}^d B_2(x_\ell) \in \mathcal{H}^{\frac{5}{2}-\varepsilon}([0, 1]^d), \varepsilon > 0, \quad (3.5)$$

by the approximated Chebyshev, cosine or transformed Fourier partial sums  $S_I^\Lambda h$  given in (2.11), (2.16) and (2.23). We study the resulting relative  $\ell_2$ - and  $\ell_\infty$ -approximation errors

$$\varepsilon_p^R(h) := \frac{\left\| (h(\mathbf{x}_j) - S_I^\Lambda h(\mathbf{x}_j))_{j=1}^R \right\|_{\ell_p}}{\left\| (h(\mathbf{x}_j))_{j=1}^R \right\|_{\ell_p}}, \quad p \in \{2, \infty\}, \quad (3.6)$$

that are evaluated at  $R \in \mathbb{N}$  uniformly distributed points  $\mathbf{x}_j \sim \mathcal{U}([0, 1]^d)$ . The approximated coefficients appearing in the approximated partial sums (2.16), (2.11) and (2.23) are calculated by solving the corresponding systems (2.17), (2.12) or (2.24).



Figure 3.2: The hyperbolic cross  $I_8^2$  (left) and its first quadrant  $I_8^2 \cap \mathbb{N}_0^2$  (right).

### 3.1 The numerical results of $\ell_2$ -approximation

Throughout this section we repeatedly use the bold number notation  $\mathbf{1} = (1, \dots, 1)^\top$  that we already used in the definition of rank-1 lattices (2.1) and expressions like  $\boldsymbol{\eta} = \mathbf{2}$  mean that  $\eta_\ell = 2$  for all  $\ell \in \{1, \dots, d\}$ .

In [23, 6, 24] we find a broad discussion on the approximation error decay of function in the Sobolev space  $\mathcal{H}^\beta(\mathbb{T}^d)$ ,  $m \in \mathbb{N}_0$ . It was proven that there is a worst case upper error bound of the form

$$\varepsilon_2 = \varepsilon_2(N, d) \approx \left\| h - S_{I_N^d}^\Lambda h \right\|_{L_2([0,1]^d)} \lesssim N^{-m} (\log N)^{(d-1)/2}. \quad (3.7)$$

In [18] we find conditions on the logarithmic and the error function transformation  $\psi(\cdot, \boldsymbol{\eta})$ , given in (2.25) and (2.26), such that a certain degree of smoothness of the given  $\mathcal{C}^m(\mathbb{T}^d)$ -function is preserved under composition with  $\psi(\cdot, \boldsymbol{\eta})$  and the resulting periodized function is at least in  $\mathcal{H}^\ell(\mathbb{T}^d)$ ,  $\ell \leq m$  and for each  $\ell$  it was calculated how large the parameter  $\boldsymbol{\eta}$  has to be chosen. According to the conditions in [18, Theorem 4], the tensorized  $B_2$ -cutoff in (3.5) is transformed into a function  $f \in \mathcal{H}^0(\mathbb{T}^d)$  of the form (2.20) for all considered torus-to-cube transformations  $\psi(\cdot, \boldsymbol{\eta})$  with parameters  $1 < \eta_\ell \leq 3$ , and into a function  $f \in \mathcal{H}^1(\mathbb{T}^d)$  for parameters  $\eta_\ell > 3$ ,  $\ell \in \{1, \dots, d\}$ . While these conditions are independent of the particular considered function  $h \in \mathcal{C}^m(\mathbb{T}^d)$ , they are pretty coarse in the sense of not catching the additional smoothness of functions like the  $B_2$ -cutoff given in (3.5) which is an almost  $\mathcal{H}^{\frac{5}{2}}([0,1]^d)$ -function as we showed earlier. In numerical tests we showcase that in certain setups the Chebyshev coefficients and the transformed Fourier coefficients will indeed decay faster than the worst case upper bound (3.7).

In dimensions  $d \in \{1, 2, 4, 7\}$  we compare the discrete  $\ell_2$ -approximation error  $\varepsilon_2$ , given in (3.6), with  $R = 1.000.000$  uniformly distributed evaluation points for all of the previously introduced approximation approaches. We consider frequency sets  $I_N^d$  for all transformed Fourier systems and  $I_N^d \cap \mathbb{N}_0^d$  for the cosine and Chebyshev systems. Both frequency sets are illustrated in dimension  $d = 2$  with  $N = 8$  in Figure 3.2. We use  $N \in \{1, \dots, 140\}$  for  $d = 1$ ,  $N \in \{1, \dots, 80\}$  for  $d = 2$ ,  $N \in \{1, \dots, 50\}$  for  $d = 4$  and  $N \in \{1, \dots, 30\}$  for  $d = 7$ .

In dimensions  $d = 1$  and  $d = 2$  we observe that the approximation errors are significantly better for  $\boldsymbol{\eta} = \mathbf{4}$  than for  $\boldsymbol{\eta} = \mathbf{2}$ , indicating the increased smoothening effect of both the logarithmic and the error function transformation. In dimensions  $d \in \{4, 7\}$ , the errors for  $\boldsymbol{\eta} = \mathbf{4}$  turn out to be worse than for  $\boldsymbol{\eta} = \mathbf{2}$ , which we suspect might be due to the increase of certain constants depending on  $\boldsymbol{\eta}$  in the error estimate (3.7). The Chebyshev approximation turns out to be a solid candidate to approximate the B-spline given in (3.5). In this specific setup, we also checked the error behavior for other parameters  $\boldsymbol{\eta} \in \{\mathbf{2.1}, \mathbf{2.2}, \dots, \mathbf{3.8}, \mathbf{3.9}, \mathbf{4.1}, \mathbf{4.2}, \dots\}$ .

transformation	$\varepsilon_2^R(h)$
(2.8) cosine system	$N^{-1.5}$
(2.13) Chebyshev system	$N^{-2.45}$
(2.25) log transf. Fourier, $\eta = 2$	$N^{-1}$
(2.25) log transf. Fourier, $\eta = 4$	$N^{-2.25}$
(2.26) error fct. transf. Fourier, $\eta = 2$	$N^{-1.9}$
(2.26) error fct. transf. Fourier, $\eta = 2.5$	$N^{-2.5}$
(2.26) error fct. transf. Fourier, $\eta = 4$	$N^{-2.5}$

Table 3.1: The observed decay rates of the discrete approximation error  $\varepsilon_2^R(h)$  as given in (3.6) when  $h$  is the univariate  $B_2$ -cutoff as defined in (3.4).

As it turns out,  $\boldsymbol{\eta} = 4$  is the best choice for the logarithmic transformation and for the error function transformation the best choice is  $\boldsymbol{\eta} = 2.5$ .

However, only the error function transformation is able to match the approximation error of the Chebyshev approximation, which also shows when we investigate and compare the error decay rates of  $\varepsilon_2^R(h)$  that were numerically observed for the univariate case  $d = 1$ . In this specific setup,  $h$  is still the continuous second-order B-spline given in (3.5) that is an element of  $\mathcal{H}^{\frac{5}{2}-\varepsilon}([0, 1]^d)$ . Hence, we expect to obtain an error decay at most  $\varepsilon_2^R(h) \lesssim N^{-\frac{5}{2}+\varepsilon}$  for any  $\varepsilon > 0$  and increasing values of  $N$  when approximating  $h$  with respect to any transformed Fourier system. We achieve these decay rates numerically with the Chebyshev system and with the transformed Fourier system when considering the logarithmic transformation with  $\eta \in \{2.5, 4\}$ . Interestingly, the decay rates of the cosine system remain at  $N^{-1.5}$ . In comparison, the logarithmically transformed Fourier system with  $\eta = 2$  loses half an order, which is slightly improved for  $\eta = 4$ . In total we observe that some transformed Fourier systems are able to achieve the same decay rates as the Chebyshev system, when we use parameterized torus-to-cube transformations  $\psi(\cdot, \eta)$  and pick an appropriate parameter  $\eta \in \mathbb{R}_+$ . The results are summarized in Table 3.1.

### 3.2 A note on $\ell_\infty$ -approximation

As derived in [18] and recalled in (2.20), the transformed Fourier system (2.21) for non-periodic functions is the result of applying an inverted change of variable  $\psi^{-1}(\cdot, \boldsymbol{\eta})$  in the form of (2.18) to the Fourier system elements within the  $L_2(\mathbb{T}^d)$ -scalar product, in order to generate another orthonormal system in a given space  $L_2([-\frac{1}{2}, \frac{1}{2}]^d, \omega)$ . There are two interpretations for the resulting integral of the form

$$\int_{[0,1]^d} \frac{\varrho(\mathbf{y}, \boldsymbol{\eta})}{\omega(\mathbf{y})} e^{2\pi i(\mathbf{k}-\mathbf{m})\psi^{-1}(\mathbf{y}, \boldsymbol{\eta})} \omega(\mathbf{y}) \, d\mathbf{y} = \int_{\mathbb{T}^d} e^{2\pi i(\mathbf{k}-\mathbf{m})\mathbf{x}} \, d\mathbf{x} = \delta_{\mathbf{k}, \mathbf{m}}. \quad (3.8)$$

We either have another periodic system of the form  $\left\{ e^{2\pi i \mathbf{k} \cdot \psi^{-1}(\cdot, \boldsymbol{\eta})} \right\}_{\mathbf{k} \in I}$  and the weighted  $L_2([0, 1]^d, \varrho(\cdot, \boldsymbol{\eta}))$ -scalar product; or we attach  $\sqrt{\varrho(\cdot, \boldsymbol{\eta})/\omega(\cdot)}$  to the individual exponentials  $e^{2\pi i \mathbf{k} \cdot \psi^{-1}(\cdot, \boldsymbol{\eta})}$  and end up with the non-periodic system (2.21) and the originally given weighted  $L_2([-\frac{1}{2}, \frac{1}{2}]^d, \omega)$ -scalar product. If we consider a constant weight function  $\omega \equiv 1$ , then there is a drawback that comes with the later choice, because  $\varrho$  is unbounded and causes singularities at the boundary points of the elements in the approximated transformed Fourier sum (2.23).

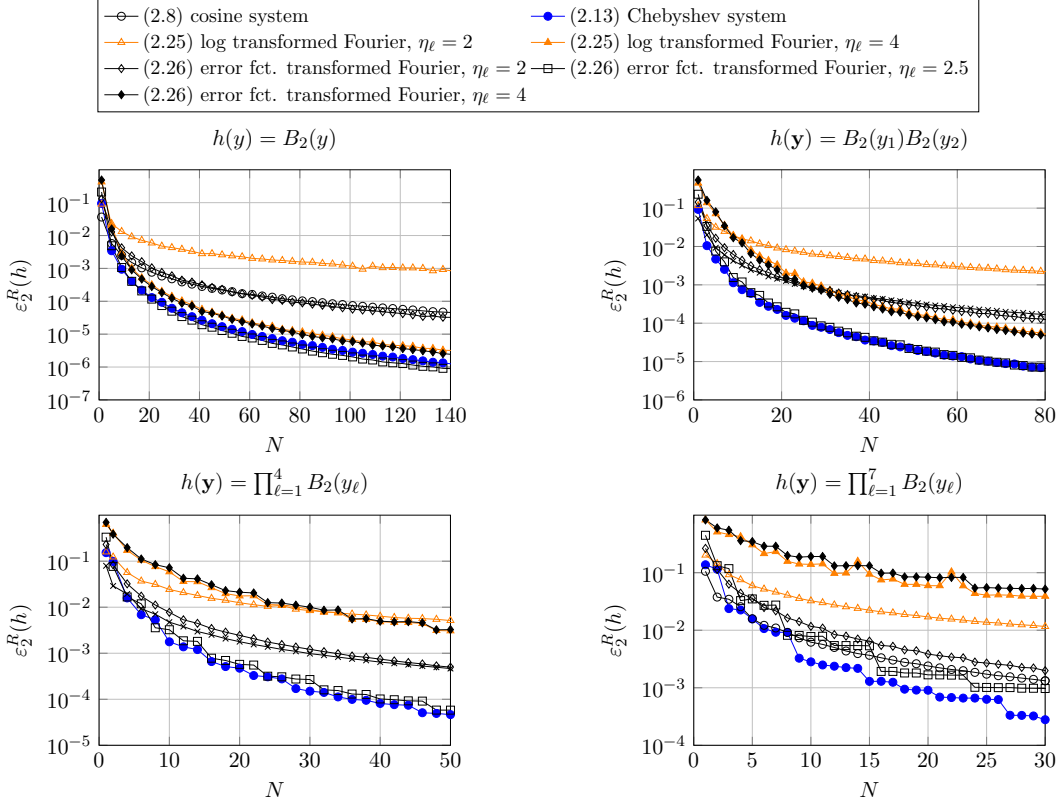


Figure 3.3: Comparing the approximation errors  $\varepsilon_2^R(h)$  of the tensored  $B_2$ -cutoff (3.5) approximated by various orthonormal systems in dimensions  $d \in \{1, 2, 4, 7\}$ .

So, the pointwise approximation error  $\varepsilon_\infty^R$  in (3.6) isn't finite, unless we consider a suitably weighted  $\ell_\infty$ -norm that counteracts the behavior of the approximant towards the boundary points, which is discussed more thoroughly in [18]. This strategy is based on choosing the weight function  $\omega$  in such a way that the quotient  $\varrho(\cdot, \boldsymbol{\eta})/\omega(\cdot)$  is either constant or converges at the boundary points. However, for any chosen torus-to-cube transformation - especially for the presented parameterized transformations  $\psi(\cdot, \boldsymbol{\eta})$  in (2.25) and (2.26) with a fixed parameter  $\boldsymbol{\eta}$  - the weight function has to be chosen in such a way so that on one hand the singularities of the density function are controlled and on the other hand the given function  $h$  is still in  $L_2([0, 1]^d, \omega)$ .

We achieve this effect for example by showing the connection of the transformed Fourier framework with the Chebyshev system, when we put the Chebyshev transformation (2.14) into the transformed Fourier system (2.21) despite the fact that it is not a torus-to-cube transformation as in (2.18). Considering the hyperbolic cross  $I_N^1$  as defined in (3.1) and  $x, y \in [0, 1]$ , we choose  $\psi$  to be the Chebyshev transformation (2.14) of the form  $\psi(x) = \frac{1}{2} + \frac{1}{2} \cos(2\pi(x - \frac{1}{2}))$ , with the inverse  $\psi^{-1}(y) = \frac{1}{2} + \frac{\arccos(2y-1)}{2\pi}$  and the density  $\varrho(y) = \frac{1}{2\pi\sqrt{y(1-y)}}$ . By putting  $\omega(y) = \varrho(y)$ , the transformed Fourier system (2.21) turns into

$$\varphi_k(y) = e^{\pi ik + ik \arccos(2y)} = (-1)^k (\cos(k \arccos(2y - 1)) + i \sin(k \arccos(2y - 1))) \quad (3.9)$$

for  $k \in \{-N, \dots, N\}$  and by combining the positive and negative frequencies we obtain

$$\varphi_k(y) = \begin{cases} 1 & \text{for } k = 0, \\ (-1)^k 2 \cos(k \arccos(2y - 1)) & \text{for } k \in \{1, 2, \dots, N\}, \end{cases}$$

which is orthogonal with respect to the  $L_2([0, 1], \omega)$ -scalar product with  $\omega(y) = \frac{1}{2\pi\sqrt{y(1-y)}}$ . With some additional scaling we obtain an orthonormal system that's equivalent to the Chebyshev system (2.13).

## 4 Conclusion

We considered the approximation of non-periodic functions on the cube  $[0, 1]^d$  by different systems of orthonormal functions. We compared the Chebyshev system that is orthonormal with respect to a weighted  $L_2$ -scalar product, the system of half-periodic cosines that uses tent-transformed sampling nodes and a parameterized transformed Fourier system. For the cosine system, which basically only mirrors a non-periodic function at its boundary points, as well as the transformed Fourier system with a small parameter, yielded the worst approximation errors. Switching to the Chebyshev system, which mirrors and additionally smoothens a given function, improved the approximation error decay. The same effect was obtained for the transformed Fourier system after increasing the parameter enough to obtain a better smoothing effect. The numerical experiments showcased the proposed parameter control in [18] that is set up by periodizing functions via families of parameterized torus-to-cube mappings. This approach in particular generalizes the idea used to derive Chebyshev polynomials.

## Acknowledgements

The authors thank the referees for their valuable suggestions and remarks. The first named author gratefully acknowledges the support by the funding of the European Union and the Free State of Saxony (ESF).

## References

- [1] B. Adcock. Modified fourier expansions: theory, construction and applications (doctoral thesis), 2010.
- [2] B. Adcock. Convergence acceleration of modified Fourier series in one or more dimensions. *Math. Comput.*, 80(273):225–261, 2011.
- [3] B. Adcock, A. Iserles, and S. P. Nørsett. From high oscillation to rapid approximation II: Expansions in Birkhoff series. *IMA J. Numer. Anal.*, 32(1):105–140, 2012.
- [4] L. Bos, M. Caliari, S. De Marchi, M. Vianello, and Y. Xu. Bivariate Lagrange interpolation at the Padua points: The generating curve approach. *J. Approx. Theory*, 143(1):15–25, 2006. Special Issue on Foundations of Computational Mathematics.
- [5] J. P. Boyd. *Chebyshev and Fourier Spectral Methods*. Dover Press, New York, NY, USA, second edition, 2000.
- [6] G. Byrenheid, L. Kämmerer, T. Ullrich, and T. Volkmer. Tight error bounds for rank-1 lattice sampling in spaces of hybrid mixed smoothness. *Numer. Math.*, 136:993–1034, 2017.

- [7] R. Cools, F. Y. Kuo, and D. Nuyens. Constructing lattice rules based on weighted degree of exactness and worst case error. *Computing*, 87:63–89, 2010.
- [8] R. Cools, F. Y. Kuo, D. Nuyens, and G. Suryanarayana. Tent-transformed lattice rules for integration and approximation of multivariate non-periodic functions. *J. Complexity*, 36:166–181, 2016.
- [9] P. Dencker and W. Erb. Multivariate polynomial interpolation on Lissajous-Chebyshev nodes. *J. Approx. Theory*, 219:15–45, 2017.
- [10] J. Dick, D. Nuyens, and F. Pillichshammer. Lattice rules for nonperiodic smooth integrands. *Numer. Math.*, 126:259–291, 2014.
- [11] T. Goda, K. Suzuki, and T. Yoshiki. Lattice rules in non-periodic subspaces of Sobolev spaces. *Numer. Math.*, 141(2):399–427, 2019.
- [12] C. Irrgeher, P. Kritzer, and F. Pillichshammer. Integration and approximation in cosine spaces of smooth functions. *Math. Comput. Simulation*, 143:35–45, 2018.
- [13] A. Iserles and S. Nørsett. From high oscillation to rapid approximation I: Modified Fourier expansions. *IMA J. Numer. Anal.*, 28:862–887, 2008.
- [14] L. Kämmerer. *High Dimensional Fast Fourier Transform Based on Rank-1 Lattice Sampling*. Dissertation. Universitätsverlag Chemnitz, 2014.
- [15] L. Kämmerer, D. Potts, and T. Volkmer. Approximation of multivariate periodic functions by trigonometric polynomials based on rank-1 lattice sampling. *J. Complexity*, 31:543–576, 2015.
- [16] F. Kuo, G. Migliorati, F. Nobile, and D. Nuyens. Function integration, reconstruction and approximation using rank-1 lattices. *Math. Comp.*, 90(330):1861–1897, 2021.
- [17] R. Nasdala and D. Potts. Transformed rank-1 lattices for high-dimensional approximation. *Electron. Trans. Numer. Anal.*, 53:239–282, 2020.
- [18] R. Nasdala and D. Potts. Efficient multivariate approximation on the cube. *Numer. Math.*, 147(2):393–429, 2021.
- [19] D. Potts and T. Volkmer. Fast and exact reconstruction of arbitrary multivariate algebraic polynomials in Chebyshev form. In *11th international conference on Sampling Theory and Applications (SampTA 2015)*, pages 392–396, 2015.
- [20] J. Shen, T. Tang, and L.-L. Wang. *Spectral Methods*, volume 41 of *Springer Ser. Comput. Math.* Springer-Verlag Berlin Heidelberg, Berlin, 2011.
- [21] I. H. Sloan and P. J. Kachoyan. Lattice methods for multiple integration: Theory, error analysis and examples. *SIAM J. Numer. Anal.*, 24:116–128, 1987.
- [22] G. Suryanarayana, D. Nuyens, and R. Cools. Reconstruction and collocation of a class of non-periodic functions by sampling along tent-transformed rank-1 lattices. *J. Fourier Anal. Appl.*, 22(1):187–214, 2016.
- [23] V. N. Temlyakov. Reconstruction of periodic functions of several variables from the values at the nodes of number-theoretic nets. *Anal. Math.*, 12:287–305, 1986. In Russian.
- [24] T. Volkmer. *Multivariate Approximation and High-Dimensional Sparse FFT Based on Rank-1 Lattice Sampling*. Dissertation. Universitätsverlag Chemnitz, 2017.